Electronic Supplementary Material (ESI) for RSC Advances.

Supporting Information

Nanocellulose supported hierarchical structured polyaniline/nanocarbon nanocomposite electrode via layer-by-layer assembly for green flexible supercapacitors

Shaoyi Lyu,[a*] Yanping Chen,[ab] Longfei Zhang,[ac] Shenjie Han,[a] Yun Lu,[a] Yuan Chen,[a] Na Yang,[a] Zhilin Chen, [a] and Siqun Wang [ca*]

[a] Research Institute of Wood Industry, Chinese Academy of Forestry, Hunan Collaborative Innovation Center for Effective Utilizing of Wood & Bamboo Resources, Beijing 100091, China.

[b] Beijing Engineering Research Center of Cellulose and Its Derivatives, School of Materials Science and Engineering, Beijing Institute of Technology, Beijing 100081, China.

[c] Center for Renewable Carbon, University of Tennessee, Knoxville, Tennessee, 37996, USA.

*Author for correspondence. Email: lvsy@caf.ac.cn (S. Lyu), swang@utk.edu (S. Wang).

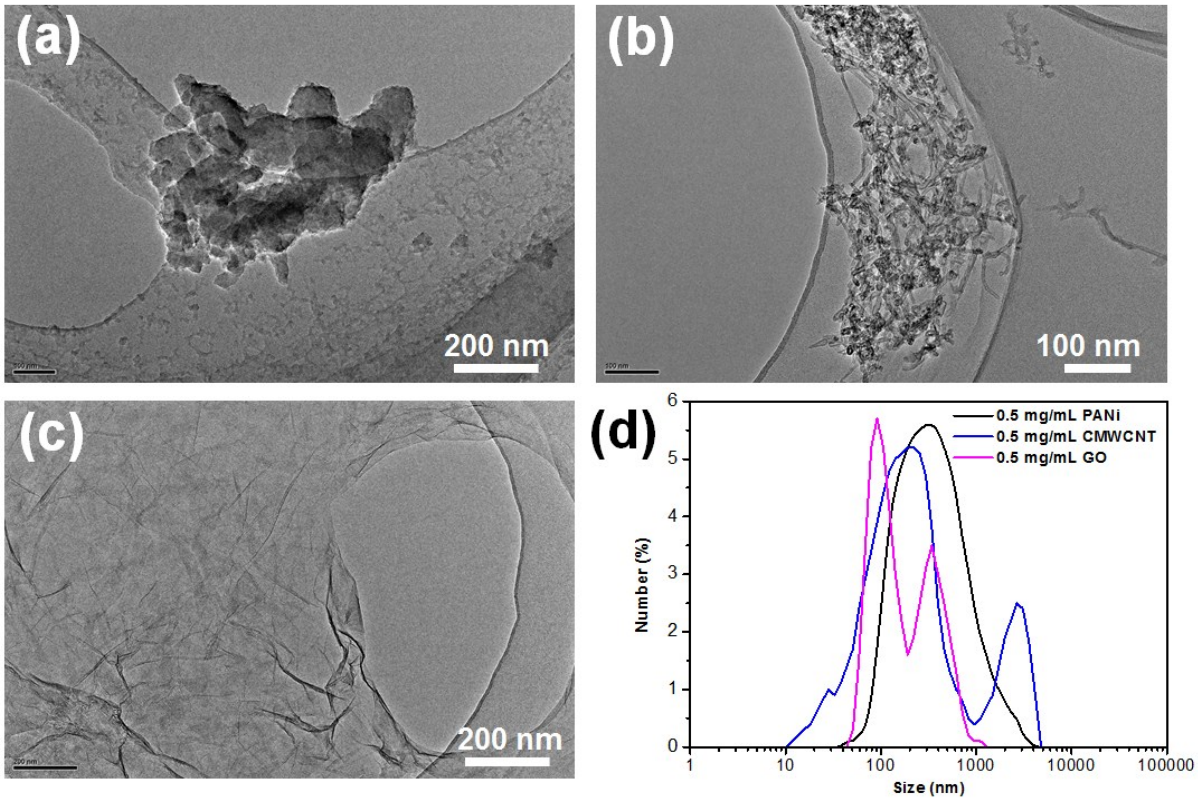

Figure S1. TEM images of (a) PANi, (b) CMWCNT, and (c) GO. (d) Particle-size distributions of PANi, CMWCNT, and GO.

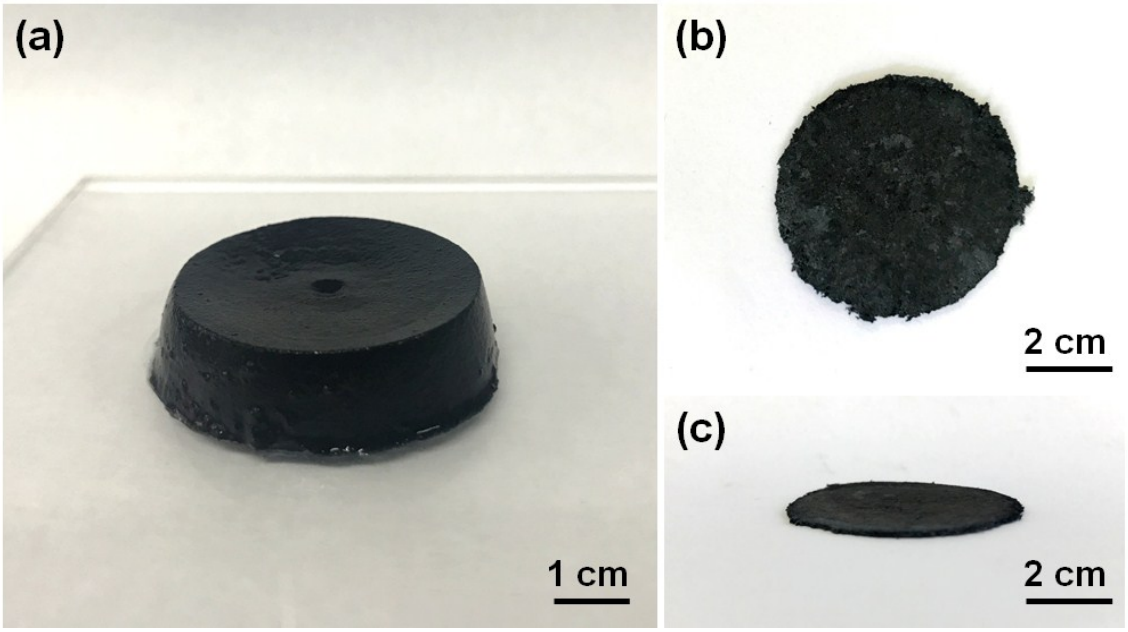

Figure S2. Representative photographic image of (a) hydrogels in wet state after assembly and (b, c) the compressed aerogel film.

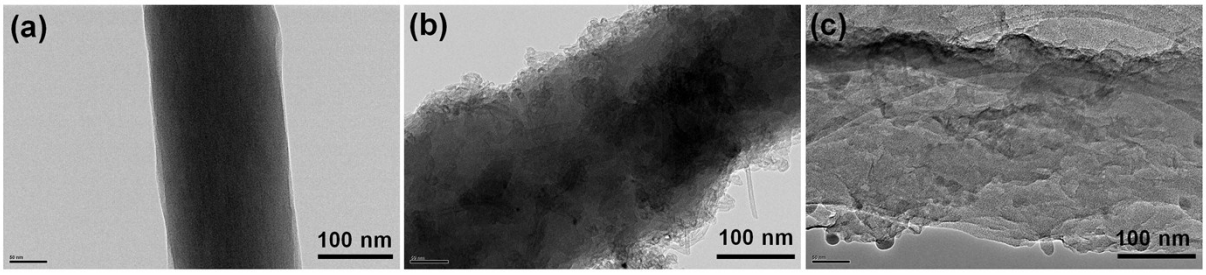

Figure S3. TEM images of (a) pure CNF nanofibril, (b) PC_{10} and (c) PG_{10} assembled on CNF nanofibril.

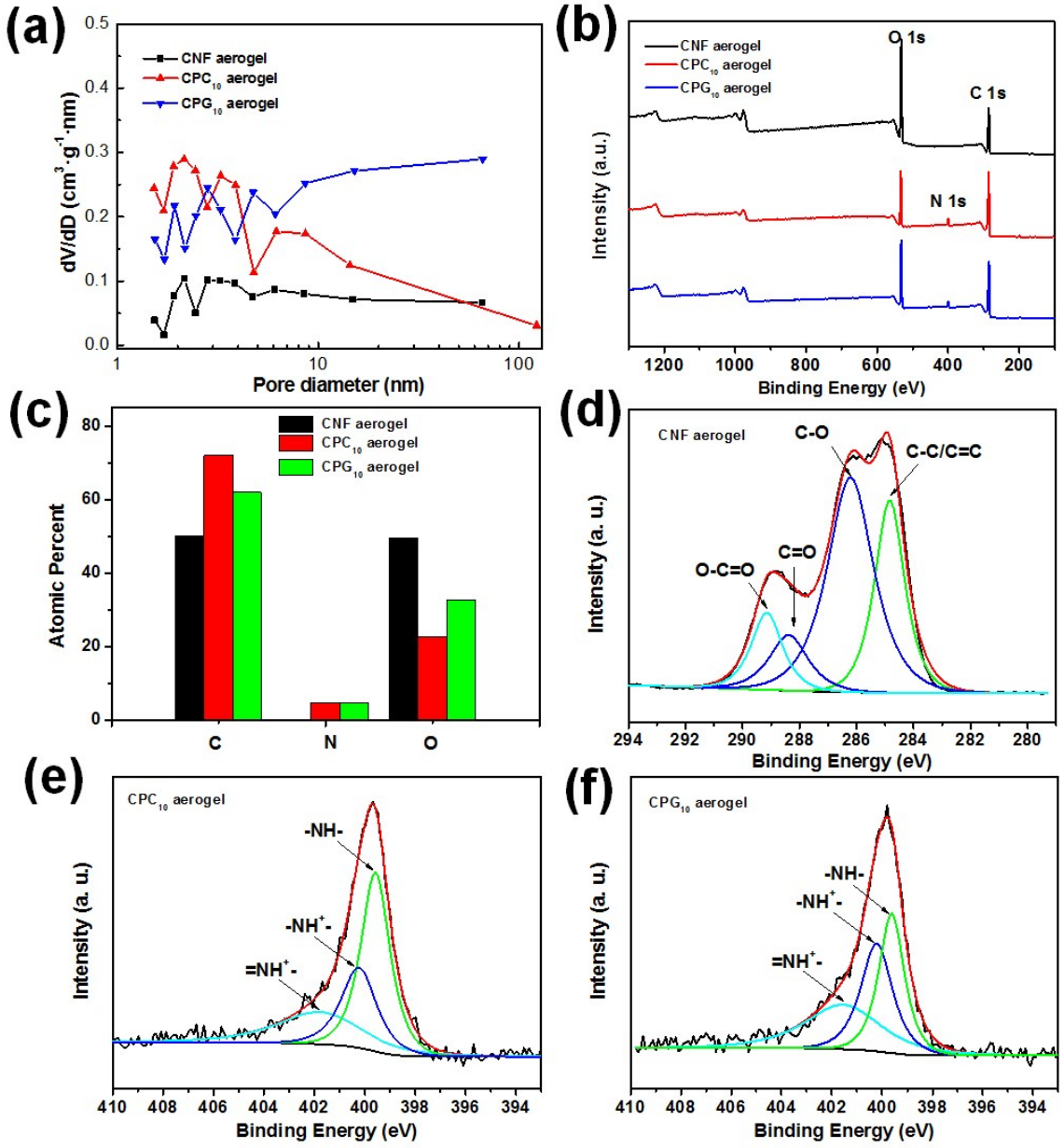

Figure S4. (a) Pore size distributions of the CNF, CPC_{10}, and CPG_{10} aerogels. (b) XPS spectra of the CNF, CPC_{10}, and CPG_{10} aerogels. (c) Atomic percentages in the CNF, CPC_{10}, and CPG_{10} aerogels. (d) High-resolution XPS C1s spectrum of the CNF aerogel, and its deconvolution. High-resolution XPS N1s spectra of the (e) CPC_{10} aerogel and (f) CPG_{10} aerogel, and their deconvolutions.

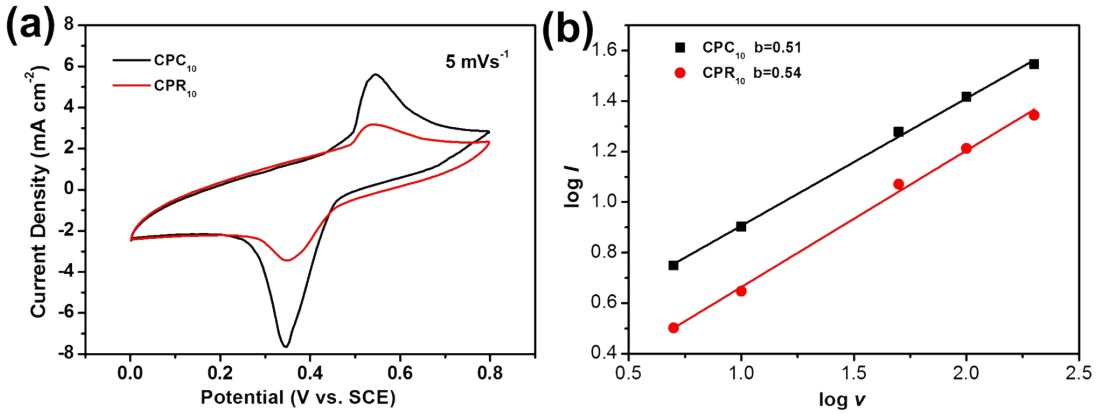

Figure S5. (a) CV curves for the CPC_{10} and CPR_{10} electrodes at a scan rate of 5 mV s^{-1} under three-electrode testing conditions in 1 M H_2SO_4. (b) Graphs of log *I* vs. log *v* for the CPC_{10} and CPR_{10} electrodes used to obtain *b* values.

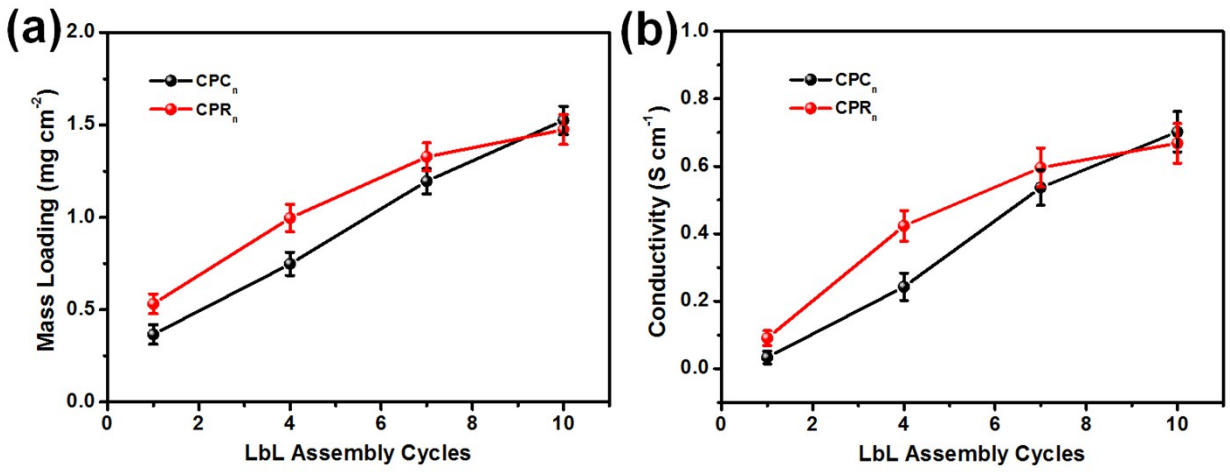

Figure S6. (a) Mass loadings and (b) conductivities of the CPC_n and CPR_n electrodes as functions LbL assembly cycles.

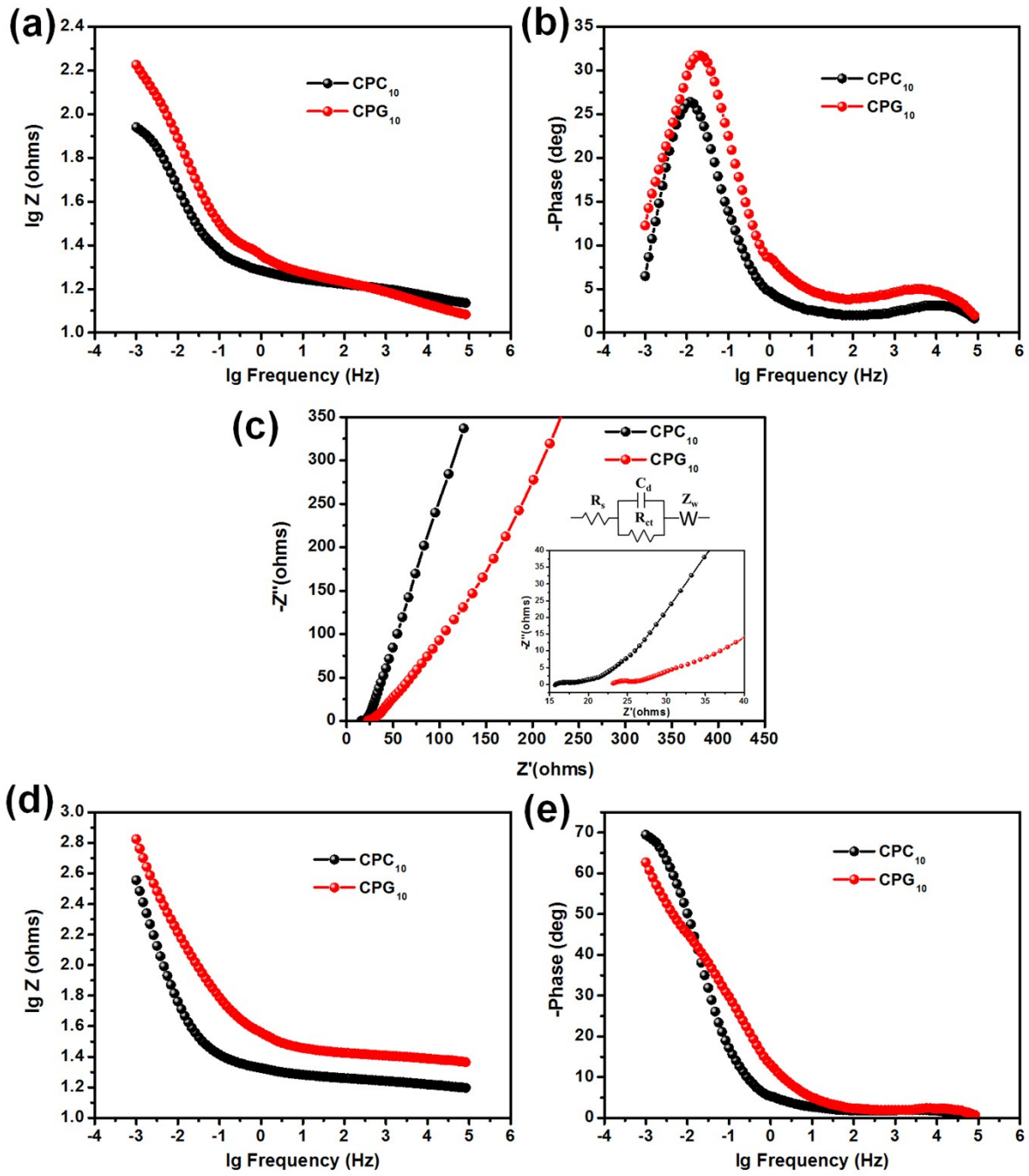

Figure S7. Bode plots of the (a) lgZ and (b) phase angle versus frequency in the three-electrode test in 1 M H_2SO_4. (c) Nyquist plots for the CPC_{10} and CPR_{10} electrodes under two-electrode test with PVA/H_3PO_4 gel electrolyte. Bode plots of the (d) lgZ and (e) phase angle versus frequency in the two-electrode test with PVA/H_3PO_4 gel electrolyte.

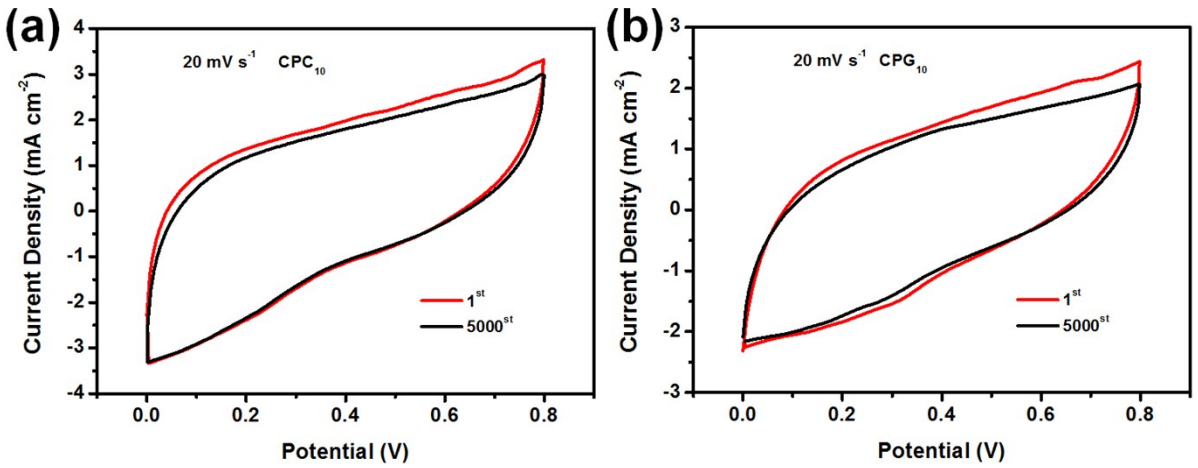

Figure S8. CV curves for (a) CPC_{10} and (b) CPR_{10} electrodes during cycle-stability testing. All data were obtained under two-electrode testing conditions with PVA/H_3PO_4 gel electrolyte.

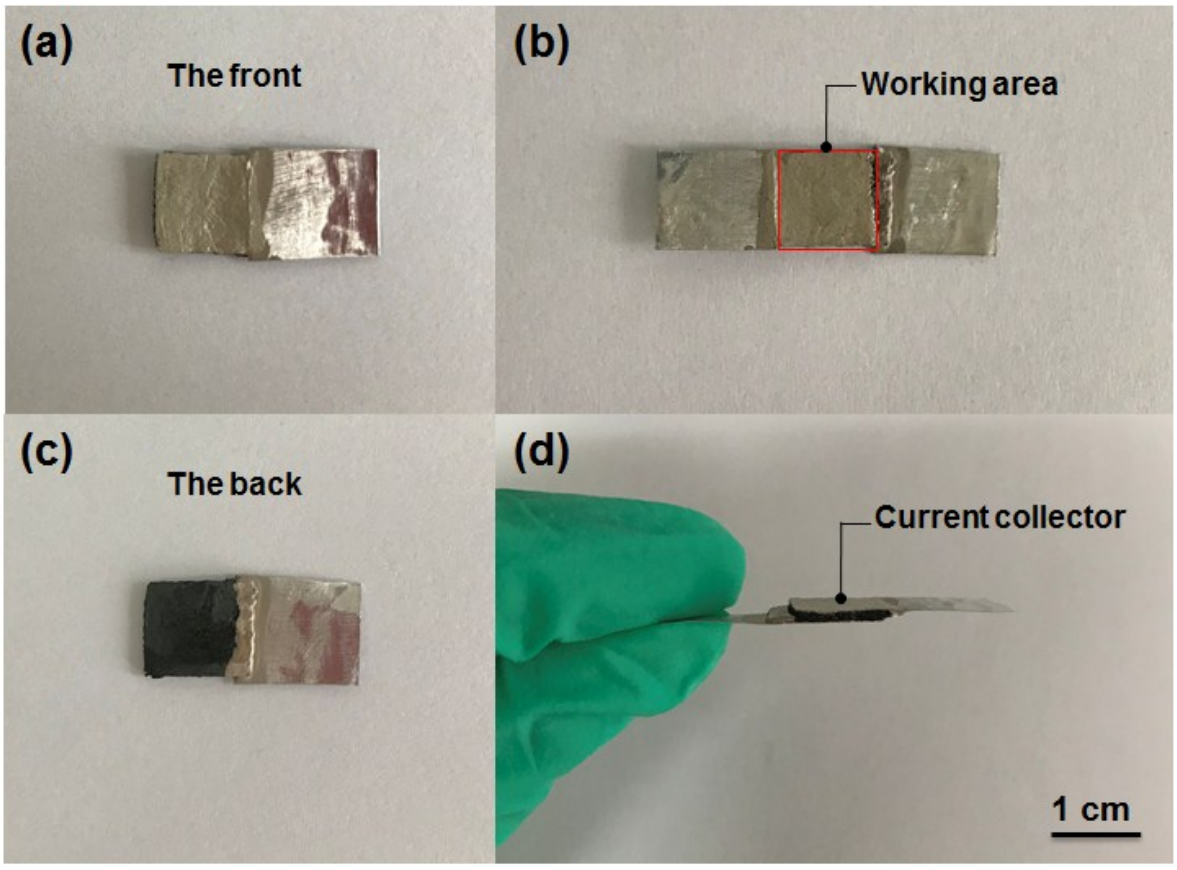

Figure S9. Optical images of the (a) front and the (c) back sides of electrodes. Optical images of supercapacitor device showing (b) working area and (d) current collector

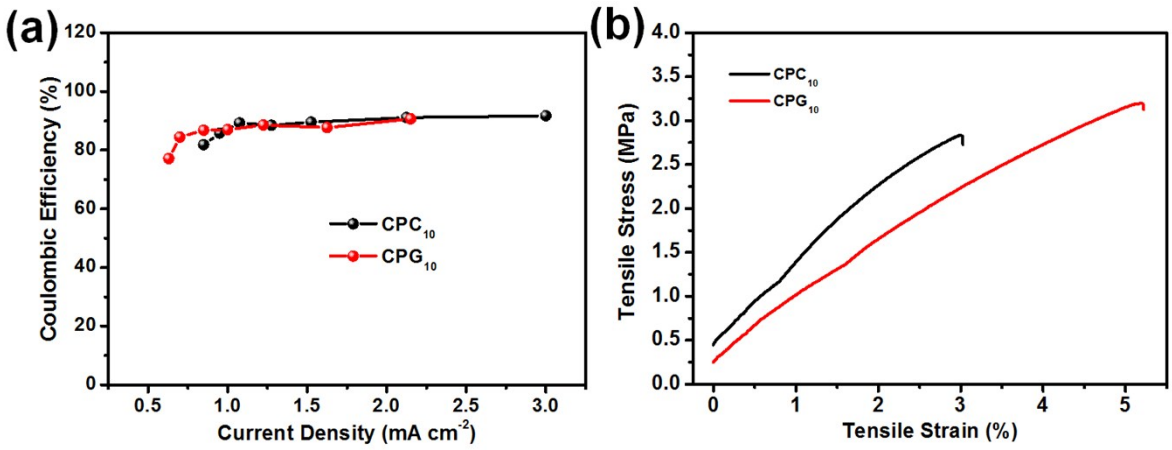

Figure S10. (a) Coulombic efficiency of the two assembled supercapacitors. All data were obtained under two-electrode testing conditions with PVA/H_3PO_4 gel electrolyte. (b) Stress-strain curves of the CPC_{10} and CPR_{10} electrodes.

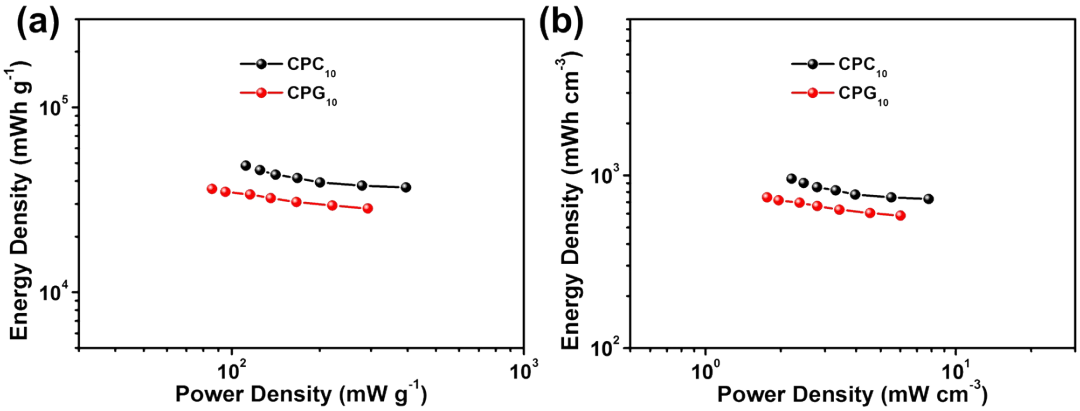

Figure S11. Ragone plots of power density vs. energy density for the two assembled supercapacitors calculated by the mass (a) or volume (b) of the device.